第32卷 第9期 焊 接 学 报 Vol. 32 No. 9
2011年9月 TRANSACTIONS OF THE CHINA WELDING INSTITUTION September 2011

真空电子束焊接35CrMnSi钢

陈国庆[1]， 张秉刚[1]， 王振兵[1]， 冯吉才[1]， 孙 毅[2]
(1. 哈尔滨工业大学 先进焊接与连接国家重点实验室，哈尔滨 150001
2. 哈尔滨工业大学 航天学院航天工程与力学系，哈尔滨 150001)


陈国庆

摘 要： 对35CrMnSi钢电子束焊接进行了研究. 结果表明，电子束焊接接头成形良好，无焊接缺陷产生. 焊缝完全奥氏体化，在随后的快速冷却后形成以板条马氏体为主，并有少量残余奥氏体的组织. 热影响区分为过热区、正火区和不完全淬火区，过热区为粗大马氏体组织，正火区为马氏体和贝氏体混合组织，而不完全淬火区为马氏体和铁素体混合组织. 接头的抗拉强度高于母材，断裂均发生在母材处，焊缝硬度显著高于母材. 接头抗弯强度为1 300 MPa，较母材有所提高，且抗弯强度随束流的增大而略有增加. 接头弯曲角为54°，较母材略有降低.

关键词： 35CrMnSi钢； 电子束焊接； 接头组织； 力学性能
中图分类号： TG456.3 **文献标识码：** A **文章编号：** 0253－360X(2011)09－0033－04

0 序 言

近年来在航空航天及其构件制造等部门，随着应用环境的不断复杂及对产品性能、寿命的要求逐渐提高，新材料和某些具有特殊性能的材料日益受到重视. 35CrMnSi是一种低合金高强度钢，属于中碳调质钢. 热处理后的35CrMnSi钢可以获得良好的综合力学性能，在保证较高的强度同时仍保有足够的韧性. 因此广泛应用于制造国内的军事装备和民用产品，主要用于制造中速、重载、高强度的零件及高强度构件，如飞机起落架等高强度零件. 高强钢的焊接性研究较广泛，常用的焊接方法有埋弧自动焊和手工电弧焊等[1,2]. 采用热量集中的脉冲氩弧焊、等离子弧焊及真空电子束等方法，有利于缩小热影响区宽度，获得细晶组织，从而提高焊接接头力学性能和抗裂性[3－6]. 电子束焊接的优势在于束斑点处功率密度高，焊缝的深宽比大，适合于厚板焊接；焊接速度快，焊缝及热影响区宽度小，焊后变形小，特别适用于精密焊接；此外，真空条件下焊接焊缝清洁度高，不易氧化，尤其对难熔及异种材料焊接具有优势[7]. 文中对35CrMnSi钢电子束焊接接头的显微组织及力学性能进行研究，为其实际应用提供理论依据.

收稿日期： 2011－07－07
基金项目： 国家重点基础研究发展计划资助项目(973)(2010CB731704)；
国家自然科学基金资助项目(51075089)

1 试验方法

试验采用的35CrMnSi钢的化学成分如表1所示. 显微组织如图1所示. 由图1可以看出，母材焊前状态为退火态，组织为珠光体和铁素体，其中珠光体为片状珠光体，片间距约为200 nm.

表1 35CrMnSi钢化学成分(质量分数，%)
Table 1 Chemical compositions of 35CrMnSi steel

C	Si	Mn	S
0.32～0.39	1.10～1.40	0.80～1.10	≤0.025

P	Cr	Ni	Cu	Fe
≤0.025	1.10～1.40	≤0.030	≤0.025	余量

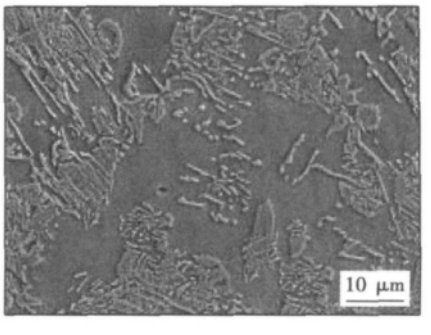

图1 35CrMnSi钢母材组织形貌
Fig. 1 Microstructure of base metal

焊接试件的厚度为2 mm，试验采用的工艺参数为加速电压55 kV，焊接束流选用范围为8～16 mA，

焊接速度为 420 ~ 510 mm/min，聚焦电流为 2 400 ~ 2 500 mA. 接头试件样品分别在光学显微镜和扫描电镜下进行组织观察，并对局部区域进行能谱分析. 抗拉强度和抗弯强度试验在电子万能试验机上进行，采用标准显微硬度计对接头金相试样进行显微硬度测试.

2 试验结果与分析

2.1 接头显微组织

35CrMnSi 钢电子束焊接性较好，熔透焊件正面的形貌如图 2 所示. 由图 2 可见，焊缝上表面宽度均匀，弧纹分布平缓，在焊透的情况下不存在咬边、焊瘤等缺陷. 但由于是薄板且为熔透焊接，在金属蒸气的反作用力和焊缝背面匙孔通道打通的共同作用下，焊缝上表面略微下凹，而焊缝根部则有熔化金属在对接面以外结晶形成凸起，焊缝横截面如图 3 所示.

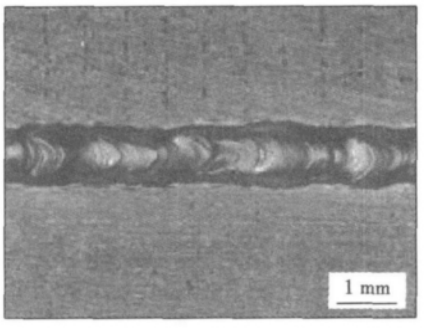

图 2 焊缝上表面形貌

Fig. 2 Appearance of weld joint

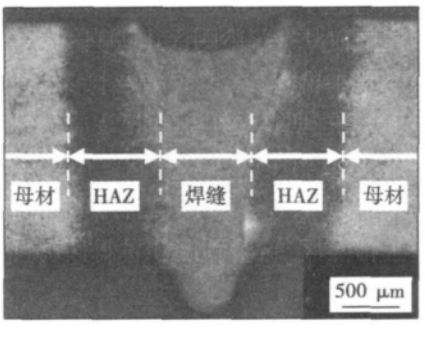

图 3 接头横截面形貌及特征区分布

Fig. 3 Macrostructure of cross section of joint

焊缝横截面为上宽下窄的锥形，焊缝平均宽度仅为 0.5 mm 左右，体现了电子束焊接热量集中的特性. 接头沿横截面可分为焊缝区、热影响区和母材三部分，其中焊缝区组织均匀，而热影响区随着距熔合线距离的增加，组织和晶粒度均发生显著变化.

图 4 所示为焊缝的微观组织，从图 4 中可以看出，焊缝组织以板条马氏体为主，并有少量残余奥氏体. 这是因为电子束焊接的热输入集中，峰值温度很高，而对于 35CrMnSi 钢这种材料，其临界温度 A_{c_3} 为 800 ℃左右，在其奥氏体化过程中，奥氏体晶粒长大速度很快，高温停留时间很短，在随后的快速冷却条件下，这种粗大的奥氏体组织过冷后形成了板条马氏体组织，但仍有少数奥氏体由于来不及转变而残留下来，从而形成了板条马氏体 + 少量残余奥氏体的组织.

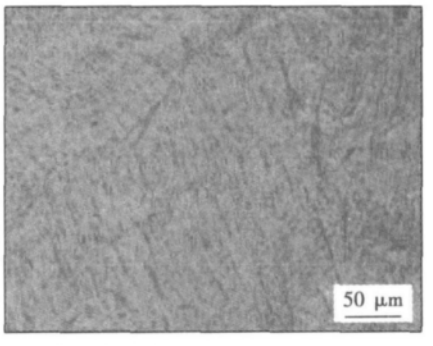

(a) 光学显微镜

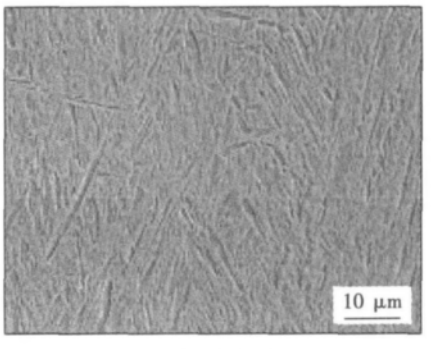

(b) 扫描电镜

图 4 焊缝微观组织

Fig. 4 Microstructure of weld joint

热影响区组织如图 5 所示，由于所受焊接热循环作用不同，热影响区不同位置的组织转变过程存在差异，从熔合线向母材方向可分为过热区、正火区和不完全淬火区. 过热区为靠近熔池部分，焊接热循环的峰值温度处于 A_{c_3} 以上，组织在加热过程中经历了奥氏体化，因而在焊接快冷后全部形成淬火组织，得到粗大的马氏体，如图 5a 所示. 而在正火区，由于冷却速度和峰值温度的不同，有部分奥氏体发生中温转变，形成贝氏体，从而形成了马氏体 + 贝氏体的混合组织，且晶粒度有所降低，如图 5b 所示. 不完全淬火区的峰值温度处于 $A_{c_1} \sim A_{c_3}$ 之间的区域，焊接加热时铁素体不发生变化，只有珠光体转变

为含碳量较高的奥氏体. 在随后的快速冷却过程中,奥氏体转变为马氏体,而铁素体形态基本不变,但有所长大. 因此,该区组织是马氏体 + 铁素体混合组织,如图 5c 所示.

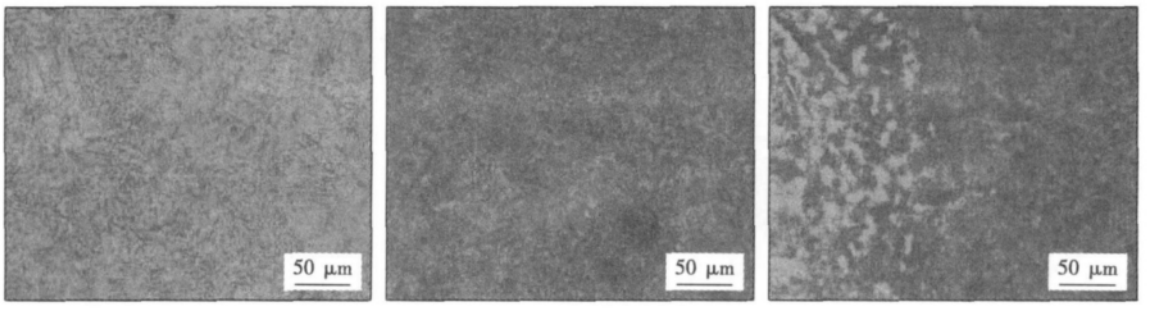

图 5　热影响区组织光学显微形貌

Fig. 5　Microstructure of heat affected zone

2.2　接头力学性能

35CrMnSi 钢焊接性较好,焊缝及热影响区没有产生明显的焊接缺陷,焊缝形成的板条马氏体组织强度和硬度较高,且塑韧性也较好,因此接头的力学性能较高. 接头抗拉强度测试结果表明,焊缝抗拉强度高于母材,拉伸试件均断裂于母材处,如图 6 所示. 对接头进行抗弯强度测试,接头抗弯强度为 1 300 MPa,较母材有所提高. 弯曲角为 54°,较母材略有降低,这与焊缝硬度大幅提高有关,母材与接头抗弯性能对比如表 2 所示.

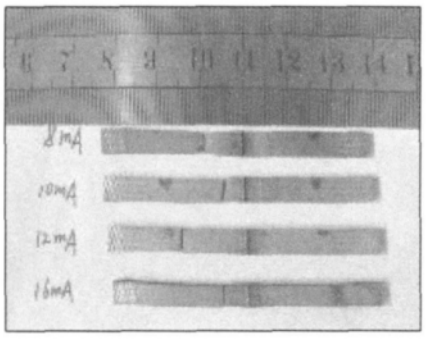

图 6　拉伸试样的断裂位置

Fig. 6　Fracture location of tensile specimens

表 2　抗弯性能对比

Table 2　Bending performance comparison

	抗弯强度 R_w/MPa	弯曲角 θ/(°)
母材	1 059.82	58
接头	1 300.93	54

典型焊接接头横截面各区的显微硬度分布如图 7所示,以焊缝中心为原点对接头单侧进行测试. 图 7 中以熔合线和热影响区与母材交界处为界线,分别标注了焊缝区、热影响区和母材区的硬度分布,其中 3 和 4 点为熔合线附近,5 点为过热区,6 和 7 点为正火区,8 点为不完全淬火区. 由图 7 可见,由于母材为退火态,而焊缝组织为板条马氏体,因而焊缝硬度显著高于母材,这也是焊后接头弯曲角要低于母材的原因所在. 热影响区中的过热区为粗大马氏体组织,因此硬度与焊缝相当. 不完全淬火区受热作用较小,硬度与母材相当. 正火区介于二者之间,形成梯度过渡.

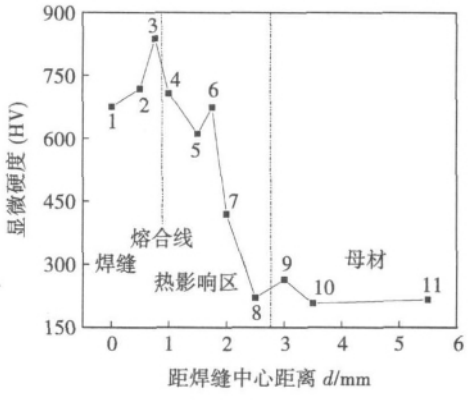

图 7　焊接接头横截面硬度分布

Fig. 7　Cross-sectional hardness distribution of welded joints

焊接热输入对接头硬度分布的影响不大,因此主要分析了焊接束流对接头抗弯强度的影响,结果如图 8 所示. 可以看出接头的抗弯强度随束流的增大而略有增加,这是因为随着束流的增加,焊缝宽度增加,有效承载面积增加,焊缝抵抗弯曲的能力增强. 但焊接束流进一步增加,熔透量过大,接头成形随之变差.

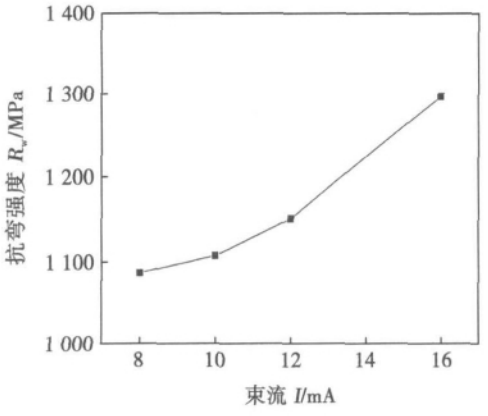

图 8 不同束流下接头抗弯强度

Fig. 8 Bending strength of joints under different beam currents

3 结 论

(1) 35CrMnSi 钢电子束焊接性较好,接头成形良好,无焊接缺陷产生. 焊缝组织以板条马氏体为主,并有少量残余奥氏体.

(2) 热影响区分为过热区、正火区和不完全淬火区,过热区为粗大马氏体组织,正火区为马氏体和贝氏体混合组织,而不完全淬火区为马氏体和铁素体混合组织.

(3) 接头的抗拉强度高于母材,断裂均发生在母材处,焊缝硬度显著高于母材.

(4) 接头抗弯强度为 1 300 MPa,较母材有所提高,且抗弯强度随束流的增大而略有增加. 接头弯曲角为 54°,较母材略有降低.

参考文献:

[1] 韩建伟, 迟永军. 大直径 BHW-35 壳体的窄间隙埋弧焊工艺[J]. 压力容器, 2004, 21(3): 32 - 35.
Han Jianwei, Chi Yongjun. Narrow gap submerged arc welding for major diametral shell made of BHW-35 [J]. Pressure Vessel Technology, 2004, 21(3): 32 - 35.

[2] 栗学治. 40MnVB 中碳调质钢的焊接[J]. 焊接技术, 1993(3): 28 - 29.
Li Xuezhi. Welding of 40MnVB quenched and tempered carbon steel [J]. Welding Technology, 1993(3): 28 - 29.

[3] 刘克强, 李志远, 刘顺洪. 超高强钢等离子弧焊接头冷弯性能分析[J]. 华中理工大学学报, 2000, 28(10): 55 - 57.
Liu Keqiang, Li Zhiyuan, Liu Shunhong. Analysis of bending property of the super high strength steel joint welded with plasma arc welding [J]. Journal of Huazhong University of Science and Technology, 2000, 28(10): 55 - 57.

[4] 吴悦计, 孙立明, 屈转利. 30CrMnSiA 钢脉冲 TIG 焊工艺研究[J]. 航天工艺, 2001(5): 11 - 13.
Wu Yueji, Sun Liming, Qu Zhuanli. Pulse TIG welding process research of 30CrMnSiA steel [J]. Hangtiangongyi, 2001(5): 11 - 13.

[5] 窦政平, 谢志强, 裴秋生. 45CrNiMoVA 钢真空电子束焊[J]. 焊接学报, 2005, 26(8): 74 - 76.
Dou Zhengping, Xie Zhiqiang, Pei Qiusheng. Vacuum electron beam welding of 45CrNiMoVA steel [J]. Transactions of the China Welding Institution, 2005, 26(8): 74 - 76.

[6] Cizelj L, Riesch H. Stresses in the first wall of a dsul-coolant liquid-metal breeder blanket during electron-beam welding [J]. Fusion Technology, 1997, 32(8): 14 - 22.

[7] 闫晓锋. 真空电子束焊在我国航空机载设备上的应用及发展趋势[J]. 航空制造技术, 2005(9): 90 - 91, 102.
Yan Xiaofeng. Application and development trend of the vacuum EB welding in airborne equipment in China [J]. Aeronautical Manufacturing Technology, 2005(9): 90 - 91, 102.

作者简介: 陈国庆,男,1972 年出生,博士,讲师. 研究方向为新材料及异种材料电子束焊接. 发表论文 20 余篇. Email: chenguoqing@hit.edu.cn

通讯作者: 张秉刚,男,副教授. Email: zhangbg@hit.edu.cn

Research on phase recognition for ultrasonic TOFD tested signal CHI Dazhao[1], GANG Tie[1], GAO Shuangsheng[1,2] (1. State Key Laboratory of Advanced Welding Production Technology, Harbin Institute of Technology, Harbin 150001 China; 2. School of Materials Science & Engineering, Shenyang Aerospace University, Shenyang 110036, China). p 17 - 20

Abstract: In ultrasonic TOFD (time of flight diffraction) tested signal, the phase information is very important parameter for qualitative identification and quantitative measurement of defect usually, Phase characteristic is not obvious in the original tested signal for the effect of testing system. For low SNR (signal to noise ratio) ultrasonic signal, the Wiener inverse filter is insufficient for improving the time resolution. To solve the disadvantuge of traditional de-convolution technique, an improved Wiener inverse filter method is proposed by employing spectral extrapolation. Computer simulated and artificial defect tested signals were processed by using traditional and improved Wiener filter technology respetively. The results showed that the proposed method could effectively improve the time resolution of the received signal, and could accurately extract the phase information about the defect tips. The proposed method could provide a reliable basis for defect identification and location.

Key words: ultrasonic TOFD; phase; Wiener inverse filter

Growth analysis of nanoparticles during plasma spraying process WANG Dongsheng[1,2], TIAN Zongjun[2], WANG Jingwen[1], DUAN Zongyin[1], SHEN Lida[2], HUANG Yinhui[2] (1. Department of Mechanical Engineering, Tongling College, Tongling 244000, China; 2. College of Mechanical and Electrical Engineering, Nanjing University of Aeronautics and Astronautics, Nanjing 210016, China). p 21 - 24, 29

Abstract: In order to optimize the processing parameters of nanostructured coating prepared by plasma spraying, the change of nanoparticle size during plasma spraying was investigated. Based on the Brook's classical theory about grain growth, a computational model for analyzing the nanoparticles growth of plasma-sprayed nanostructured agglomerated ZrO_2-7% Y_2O_3 powders was established. The effects of the thermal circulation curve and nanoparticle diameter on grain growth were studied. Meanwhile, experiment of plasma spraying using nanostructured agglomerated powders was carried out. The results showed that the nanostructured coating had a bimodal microstructure, which was composed of both fully melted regions and partially melted regions. The partially melted regions were composed of slightly grown-up nanoparticles. The obtained experimental results showed a good agreement with the calculated results, which indicated that the nanoparticles growth theory based on the Brook's theory was correct and reliable. The theory provides theoretical basis for nanoparticles growth of plasma spraying.

Key words: plasma spraying; nanostructured agglomerated powders; nanoparticles growth

Welding process and joint properties of hybrid welding on 2219 aluminum alloy RAN Guowei, SONG Yonglun, YAN Sibo, LIN Jiangbo (Department of Mechanical Engineering & Applied Electronics Technology, Beijing University of Technology, Beijing 100124, China). p 25 - 29

Abstract: The correlation between three welding processes and joint microstructure as well as properties was investigated on 2219 aluminum alloy of 6 mm thickness. The three welding processes were TIG welding with filler wire, low-power laser assisted TIG hybrid welding and laser high-frequency pulse TIG hybrid welding respectively. The results showed that, compared with the TIG welding, the hybrid welding processe could improve the welding speed, reduce the heat input significantly, refine the microstructure of the joint, and reduce the width of eutectic α (Al) + θ (CuAl2), especially eliminate the porosities of fusion zone effectively. Furthermore both the joint properties and stress corrosion resistance were improved significantly. The average fracture time for 2219 aluminum alloy through the laser high-frequency pulse TIG hybrid welding was significantly longer than that through the TIG welding, which was about 93% of the average fracture time for 2219 base material.

Key words: aluminum alloy; hybrid welding; joint properties

Wetting correlations between rosin & other flux components and Sn-9Zn/Cu MENG Gongge, ZHANG Hongyan, LIU Chao, GU Baisong (School of Material Science & Engineering, Harbin University of Science and Technology, Harbin 150040, China). p 30 - 32

Abstract: Wetting correlations between rosin & other 6 flux components and Sn-9Zn/Cu are studied based upon uniform design method. The factors rosin, $ZnCl_2$, NH_4Cl, ethylene glycol, oleic acid and lactic acid, were divided into three groups and twelve levels in the experiment. By using computer software UST4.0, the wetting spread area were processed statistically and three correlative equations were obtained. The results showed that the effect of $ZnCl_2$, oleic acid and the mutual term of $ZnCl_2$ & NH_4Cl were positive. The effects of NH_4Cl was negative, and that of rosin with $ZnCl_2$ or NH_4Cl together is little, $ZnCl_2$ or oleic acid is also in quadratic & negative form. The analysis of variance showed that the multinomial equations were sound and meaningful.

Key words: wetting; flux; tin-zinc solder; uniform design; correlations

Vacuum electron beam welding of 35CrMnSi steel CHEN Guoqing[1], ZHANG Binggang[1], WANG Zhenbing[1], FENG Jicai[1], SUN Yi[2] (1. State Key Laboratory of Advanced Welding Production Technology, Harbin Institute of Technology, Harbin 150001, China; 2. Faculty of Astronautical Engineering and Mechanics, School of Astronautics, Harbin Institute of Technology, Harbin 150001, China). p 33 - 36

Abstract: The electron beam welding of (35CrMnSi steel) was studied. The results showed the appearance of electron beam welded joint was good, and no welding defects were found. The weld was fully austenitized, the rapidy solidified microstructure mainly consists of batten martensite while a small amount of residual austenite. The heat-affected zone can be divided into the overheated zone, normalized zone and slack quenching zone. The microstructure of overheated zone was coarse martensite. The microstructure of normalized zone was the mixture of martensite and bainite. The tensile strength of joint was higher than the base metal and the fracture occurred at the base metal. The weld hardness was significantly higher than the base metal, the bending strength was 1 300 MPa, which was better than base metal, and the bending strength increased slightly with beam current. The bending angle of joint was 54°, which was slightly lower than the base metal.

Key words: 35CrMnSi steel; electron beam welding; microstructure; mechanical properties

Effects of metal activating fluxes on A-TIG welding of magnesium alloy ZHANG Zhaodong, CAO Quanjin (Key Laboratory of Liaoning Advanced Welding and Joining Technology, School of Materials Science and Engineering, Dalian University of Technology, Dalian 116024, China). p 37 - 40

Abstract: Four kinds of metal cadmium, znic, titanium and chromium were used as the activating fluxes for the A-TIG welding of magnesium alloy and the influence of metal activating fluxes on the weld morphology, the arc shape and the arc voltage has been analyzed. The results indicated that compared with the conventional TIG welding, both znic flux and cadmium flux increased the weld penetration depth, while the chromium flux reduced it and the effect of Ti flux was negligible. It could also be observed that the arc concentrated and the arc voltage increased with both znic and cadmium fluxes, while the variations of the arc and the arc voltage with titanium and chromium fluxes were hardly be observed. The main mechanism that znic and cadmium activating fluxes enhance weld penetration for the A-TIG welding of magnesium alloy may be that these fluxes constrict the current-conducting channel of the arc during the positive period of alternating current, due to the effect of the melting point, the boiling point and the first ionization energy.

Key words: magnesium alloy; activating flux; metal; A-TIG welding

Research on wear resistance of compound material surfacing alloy with high vanadium content ZONG Lin[1,2], LIU Zhengjun[2], GAO Hailiang[2], LI Lecheng[2] (1. School of Mechanical Engineering, Shenyang University of Chemical Technology, Shenyang 110142, China; 2. School of Material Science and Engineering, Shenyang University of Technology, Shenyang 110870, China). p 41 - 44, 48

Abstract: In order to study the wear resistant composite material with high Vanadium content, Fe-Cr-V-C alloy system was designed with plasma arc surfacing. The mechanical properties of surfacing overlays were examined with Rockwell hardometer and wear testing machine respectively. The phase composition, shape and distribution of microstructure have been researched by XRD, OM and SEM. The results showd that the mechanical properties of the surfacing overlay improved with the increasing of vanadium content. When the vanadium content was up to 26.2 percent, the mechanical properties of surfacing overlay obtained optimum value, the hardness was 64.9 HRC and the wear loss was 0.078 4 g. The numbers of vanadium carbide increased with the increasing of vanadium content. vanadium carbide particles diffused in the martensite matrix and formed wear resistant structure with $(Fe,Cr,V)_7C_3$ which distributed along grain boundaries. In a word, the property of wear resistance of surfacing overlay is very good.

Key words: surfacing alloy; plasma arc; surfacing; wear resistance

Feature extraction and image processing for underwater weld with laser vision LIU Suyi, LI Bing, ZHANG Hua, JIA Jianping (Robot and Weld Automation Key Lab., Nanchang University, Nanchang 330031, China). p 45 - 48

Abstract: Automation and intelligence are the development direction for underwater welding, and real-time sensing and detecting of underwater weld position is a key technology, among which laser vision sensing is a good-prospect detecting method. Noise features of weld image under different water environment and underwater V-groove weld image pre-processing are discussed. And both the application of mean shift algorithms on underwater weld image segmentation and linear Hough transform on extracting image features of underwater weld are studied. Experiment results show, after image enhancement and filtering, laser stripe including weld features could be effectively segmented with mean shift algorithms, and linear Hough transform was suited for precisely extracting V-groove weld feature points on the basis of thinning images.

Key words: feature extraction; image segmentation; underwater weld; laser vision

Ultrasonic testing technology of weld defect based on video positioning HU Wengang, GANG Tie, WANG Jinhai (State Key Laboratory of Advanced Welding Production Technology, Harbin Institute of Technology, Harbin 150001, China). p 49 - 52

Abstract: Manual ultrasonic testing system of weld defects based on video positioning of USB camera was studied. The planar position of ultrasonic probe relative to the weld bead was obtained by USB camera, and the depth of weld defects was obtained by ultrasonic probe. Then the locational qualitative and quantitative analysis on weld defects was obtained by the method of three-view projection imaging technology intuitively. This system is applicable to the field test of welded structure on service. Ultrasonic testing was performed to the actual weld, including crack defect by this system. The result showed that the location, size and distribution of weld defects could be characterized conveniently, quickly and intuitively, and the method was helpful for the qualitative recognition of different weld defects.

Key words: ultrasonic testing; weld defect; video positioning; projection imaging

Study on arc length control system for pulsed MIG welding of aluminum alloy LU Lihui[1], FAN Ding[2], HUANG Jiankang[1], ZHU Ming[1], SHI Yu[2] (1. Key Laboratory of Non-ferrous Metal Alloys and Processing, The Ministry of Education, Lanzhou University of Technology, Lanzhou 730050, China; 2. State Key Laboratory of Gansu Advanced Non-ferrous Metal Materials, Lanzhou University of Technology, Lanzhou 730050, China). p 53 - 56

Abstract: Research work of wire extension control based on vision sensing was done in pulsed MIG welding process of aluminum alloy. A rapid prototyping control platform was established for pulsed MIG welding of aluminum alloy using real-time target environment based on xPC. With vision sensing of welding zone image and corresponding image processing algorithm, a fuzzy PID closed loop control system for wire extension was designed on the basis of the built rapid prototyping control platform. Then experimental results showed that the method of vision sensing could meet the control requirements of wire extension stability, the rapid prototyping control system built with fuzzy PID controller based on vision sensing could realize the well control of the wire extension in pulsed MIG welding of aluminum alloy and also had strong robustness and quick response ability.

Key words: sliding mode controller; rapid prototyping;